THERMAL AND MECHANICAL DESIGN OF THE EXPERT C/C-SIC NOSE

T. Reimer[(1)], T. Laux[(1)]

[(1)]DLR, Institute of Structures and Design, Stuttgart, Germany

ABSTRACT

The EXPERT mission will be carried out as a sub-orbital flight of the EXPERT vehicle reaching a velocity of 5 km/s. The vehicle is designed as an aerodynamic probe to gather in-flight data concerning the aerothermodynamic environment of re-entry vehicles. For that purpose, scientific payloads are measuring in the very front of the vehicle but also right up to it´s base. Since the quality of the data is depending on an undisturbed flowfield, the choice was made for a nosecap of C/C-SiC, a ceramic matrix composite that can withstand the heat loads in the stagnation area very well. Another aspect of selecting a C/C-SiC nose concerns the fact that it is also the carrier structure for a number of sensors that have to be integrated structurally. The loads acting on the nose are severe, with heat loads up to 1.5 MW/m² and simultaneous pressure of more than 150 kPa as well as a deceleration load of 17g. The German Aerospace Center (DLR) in Stuttgart will manufacture the cap. The paper describes the thermal and mechanical design of the nose after adjustment to the latest set of loads.

1. INTRODUCTION

The EXPERT (European eXPErimental Re-entry Testbed) project conducted by the European Space Agency (ESA) aims at improving the understanding of aerothermodynamics during the return of space vehicles because there has been little data so far gathered in Europe in re-entry missions. The EXPERT vehicle is a ballistic capsule as depicted in Fig. 1 and has a length of 1.55m and a base diameter of 1.2m.

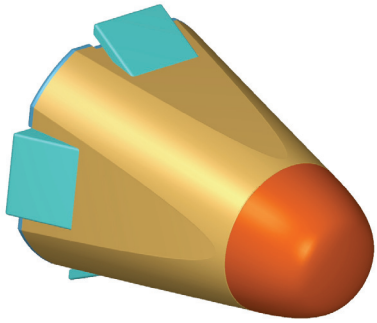

Figure 1: The EXPERT vehicle.

The goal of the mission is not just a re-entry technology demonstration, but to collect data that is related to the physical phenomena of a high-temperature flowfield. For that reason a number of scientific payloads will be integrated into the vehicle. Many decisions in the design process were taken on the basis of being in accordance with the data collecting and not disturbing the flow environment. That is of concern especially in the front of the vehicle where the heat shield has to fulfil these additional considerations on top of the thermal protection function. Therefore, the system configuration excluded ablative types of thermal protection from the vehicle system from the beginning, since they can not meet the requirement of minimizing flow contamination and contour stability. With these restrictions on the possible selection of materials, the choice was quickly narrowed to a CMC system using the C/C-SiC material from DLR.

2. CMC MATERIAL CHARACTERISTICS

The peak heat load for EXPERT is relatively large and usually would lead to the choice of ablative materials for the TPS. However, in this case there were additional issues to consider. Most important were the case of geometric stability of the aerodynamic contour and the issue of chemical pollution of the flowfield. Contour stability is important because the flow shall remain as much undisturbed as possible, which also means a late transition from laminar to turbulent. Chemical pollution of the flow with ablated material would impact a number of payloads on board that measure the chemical composition of the flow. These considerations led to the selection of a CMC material system for the nose of the vehicle.

Although the C/C-SiC material is used mainly in technology developments for re-usable space transportation systems, the use for the nose of EXPERT is also very well justified. Usually C/C-SiC can be regarded as a fully re-usable material up to temperatures of approximately 1600°C. In the case of EXPERT, temperatures will be as high as 1900°C, however, the slow surface erosion process that will be starting is several orders of magnitude smaller than for traditional ablators.

The quantitative effect of the surface erosion was estimated in [1] for the different types of trajectory that were planned. For the 5 km/s mission which will be flown these estimations predict a total surface mass loss of 0.13 kg/m² in the stagnation area which translates into a

thickness decrease of 0.07 mm which is almost neglectable.

Also the issue of the passive to active oxidation transition of the C/C-SiC material is affected slightly by the new load data for the first mission. Due to the increased mass of the vehicle from 350 kg to 397 kg, the entry trajectory with the physical parameters of temperature and pressure is also somewhat different from the originally planned one of 5 km/s.

The C/C-SiC material shows a typical oxidation characteristic which can be observed for all CMC materials of that type which are silicon based carbon fibre reinforced. Oxidation of the carbon fraction of the material starts at roughly 450°C but can be reduced very much by the use of appropriate oxidation protection layers, like CVD-SiC. Unfortunately silicon carbide shows a specific oxidation behaviour due to the oxidation characteristics of both silicon oxides SiO and SiO_2.

The formation of SiO_2 is termed as passive oxidation, whereas the term active oxidation is used when SiO is formed. The transition from passive to active oxidation is mainly dependent on high temperatures and low oxygen partial pressures. Besides the mass loss, the active oxidation in dissociated environments is accompanied by a sudden temperature increase of up to 500K [2].

During the aerothermodynamic design of the mission trajectories there was a relatively big emphasis on the question whether the nose of the vehicle will pass from passive oxidation into the active oxidation regime and some effort was undertaken to stay away from the active regime. However, it has to be stated that there is no clearly distinguishable border that separates these regimes from each other, rather there is a transition zone in which transition may happen. Test results in various facilities and with different types of materials support this view. Therefore, the trajectories for EXPERT were looked at from that point of view.

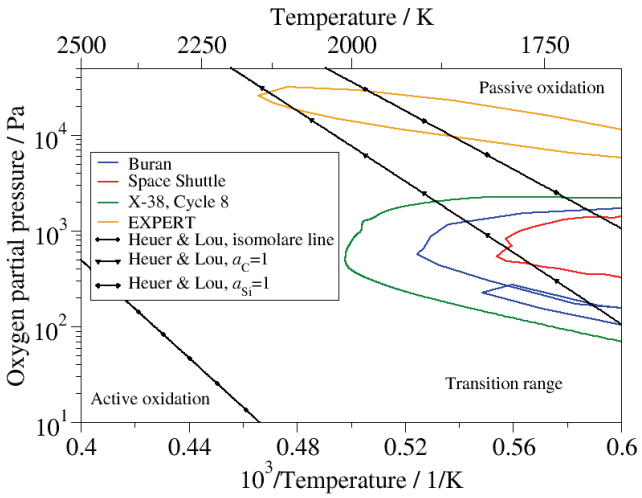

Figure 2: EXPERT trajectory in the transition regime.

Fig. 2 is a graphical description of that issue where the transition area is based on thermodynamical considerations of relevant reactions [2] with trajectories for the Shuttle, Buran and X-38 for comparison [3-5]. It can be seen that even for the first mission transition might occur, however, it is now even closer to the boundary of the transitional region and thus more unlikely. If transition starts it would be a great opportunity to collect flight data of the effect.

3. LOAD ENVIRONMENT

The aerodynamic environment for the vehicle during re-entry is typical for a ballistic flight into earth atmosphere from low earth orbit with a relatively small capsule. The EXPERT project intended to go with a step-by-step increase of the entry velocity for consecutive missions where it was planned to conduct a first flight with a sub-orbital velocity of 5 km/s and then go for higher speeds up to 7 km/s in further flights. At present, however, the planning, and thus the design process, was reduced to one mission with the initial 5 km/s speed.

Table 1: EXPERT mission 1 key reference data.

Entry speed	5000 m/s
Entry angle	-5.5°
Vehicle mass	397 kg

The latest set of loads was derived for a mission with the rererence data given in Table 1. Most important for the design of the nose of the vehicle are the peak heat load at 1.43 MW/m² for the stagnation area and the peak dynamic pressure of 149 kPa which are shown in Fig.3. These peak loads occur with only 10 seconds difference in time during the flight, with the peak heat load preceding. So, when the time lag of the temperature due to the capacity effect of the thermal structures is considered, peak temperature and maximum pressure will be reached practically at the same time. The load factor as a result of the pressure increase is shown in Fig. 4.

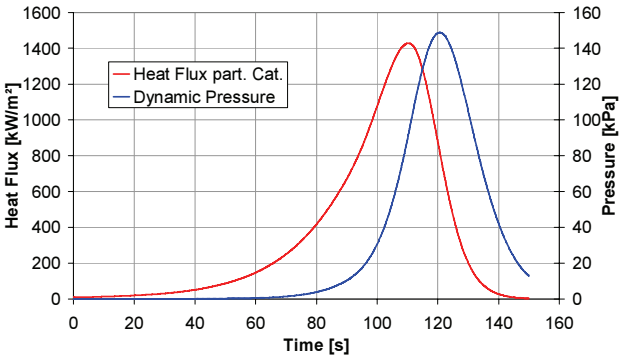

Figure 3: Stagnation heat flux and dynamic pressure.

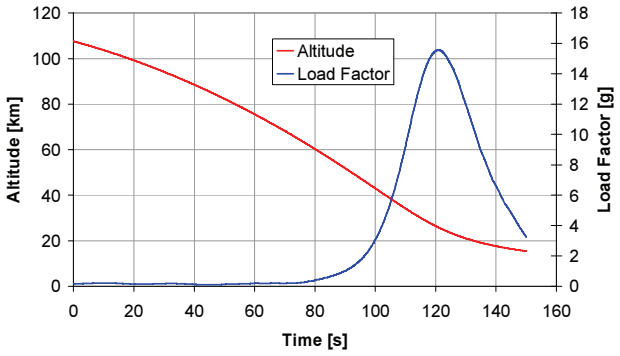

Figure 4: Altitude and load factor.

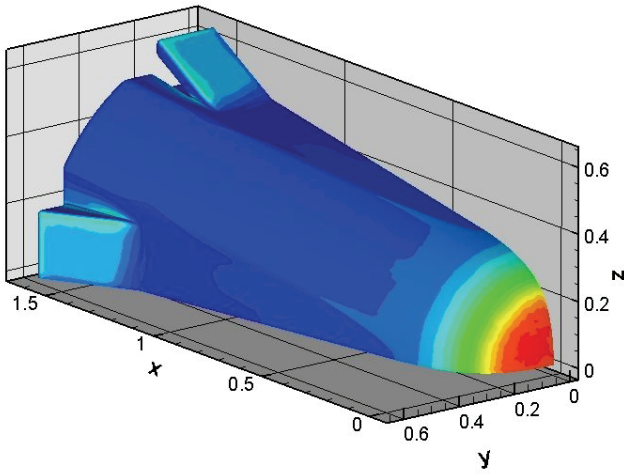

Figure 5: Schematic EXPERT heat flux distribution.

The heat load distribution over the nose is illustrated schematically in Fig. 5. In Fig. 6 the heat flux is plotted against the nose radius and it can be noted that over the front region of the nose the value of the heat flux is almost constant up to the start of the bend where the curvature of the nose increases. From the bend up to the edge of the nose the heat flux is decreasing rapidly with a small bump about halfway between bend and edge.

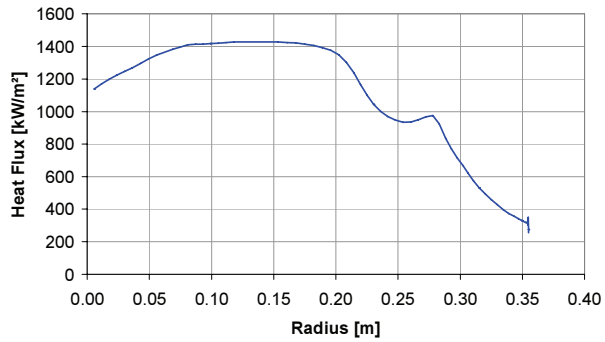

Figure 6: Heat flux over the nose radius.

4. NOSE DESIGN TRADE-OFF

The design of the nose for the EXPERT capsule is mainly concerned with the design of the load introduction into the nose shell. The pressure load as the dominating mechanical load is acting mainly on the front region of the nose in axial direction and so, the shell itself is very stiff due to it´s bell shape. The wall thickness was selected with a value of 6mm and not optimized for minimum mass, in part for manufacturing reasons and because the C/C-SiC shell itself makes up for only about 20 – 25% of the total nose assembly mass.

The phase B investigations were based on the approach of an attachment system that was used for the X-38 nose as illustrated in Fig. 7. That system was developed, however, with the requirements of a long-duration re-entry of a lifting body with sustained high temperatures along the border of the material re-usability limits for about 10 minutes. In contrast, mechanical loads were much less than for EXPERT. Therefore, the X-38 attachment system was designed for high temperatures spreading into the attachment components some of which were manufactured also from C/C-SiC [6].

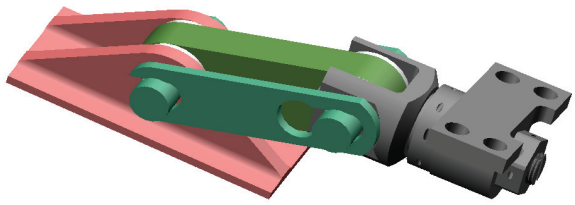

Figure 7: X-38 attachment design.

In the case of EXPERT the situation is different. Stagnation temperatures are in fact higher than for X-38 but only present for a short time and the areas near the attachment locations are subjected to far less heat loads. On the other hand the mechanical load on the nose is about 7 times the one of X-38. The results for the initially selected X-38 attachment design indicated that the stiffness in lateral direction was not high enough to meet the required stiffness of a minimum of 90 Hz for the first Eigenfrequency (EF).

In addition, the thermal analysis during phase B indicated that the temperatures at the downstrem edge of the nose could be expected to be low at around 1000 K in comparison to the stagnation point values of over 2500 K (that value was obtained still for the faster entry speeds). In view of these results the motivation for the X-38 attachment system was reduced.

Another issue was that due to the low temperatures at the edge in the case of EXPERT, also the

thermal expansion of the nose diameter at the edge is reduced. That is important because the attachment must not restrict the expansion to avoid the creation of stresses due to the restricted movement which was an issue for the X-38 system that can follow the expansion due to it´s double bolt joint design. For these reasons, after a first round of detailed investigations of the attachment systems under the EXPERT loads, the decision was made to switch to a different attachment design better suited the load environment.

Therefore, a comparative analysis with a different design approach was carried out and showed that a better stiffness can be achieved, leading to higher values for the eigenfrequencies of the nose. The design variant is shown in Fig. 8 using thin brackets of metal to fix the nose to the cold structure which is named “colander” in the following.

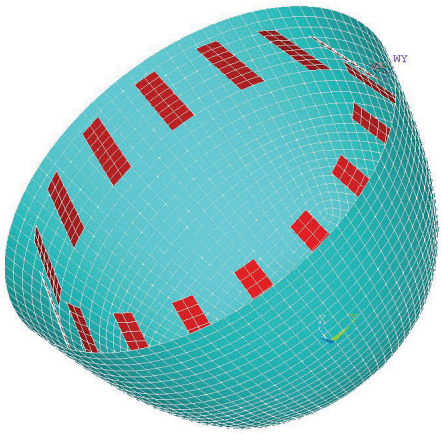

Figure 8: Alternative attachment design model.

To simplify the analysis it was assumed that the brackets were fixed directly to the nose and the colander. The results indicated that with such a system and an increased number of brackets the stiffness could be increased considerably. The thermal expansion of the nose diamater at the edge is handled by elastic deflection of the brackets.

The brackets are oriented in such a way that they are in compression when the pressure load acts on the nose. In principal they could also be oriented the other way round to have them under tension, which would prevent any issues related to buckling. However, that would move the fixation of the attachment brackets to the internal cold structure away from the nose edge and would interfere with some of the sensors mounted to the cold structure in the nose. For that reason the orientation with the brackets under compression was preferred. It also has the bracket ends stick out over the edge of the nose which gives good access for installation purposes.

During phase B the X-38 system was analysed with a variation of the lever cross section properties. These results are stated in Table 2. The cross section was varied within reasonable boundaries, but the 1. EF remained below 130 Hz.

Table 2: X-38 attachment type analysis.

Eight attachments, length=80mm, angle=40° to vehicle x-axis, colander aluminum			
Colander thickness [mm]	Lever height [mm]	Lever width [mm]	Lowest Eigenfreq. [Hz]
5	25	12.5	129
5	20	10	95
5	15	10	83
5	10	6	34
3	20	10	91
3	15	10	80
8	20	10	97
8	15	10	84

With the bracket system the EF could be raised considerably up to 200 Hz and even more, depending on the number of brackets and their geometry. The relation between the number of brackets and the EF is almost linear when equal thickness and material are compared. Table 3 shows an overview of the influence of the bracket numbers and material. The thickness of the colander has an influence on the overall system stiffness but it is confined to the immediate fixation region of the brackets which can be seen in Table 4. When the colander structure is totally removed ahead of a location of x equal to 0.37 m in the vehicle system, there is no influence on the overall stiffness.

Table 3: Metallic bracket type analysis.

Brackets	Bracket thickness [mm]	Bracket material	Lowest Eigenfreq. [Hz]
24	2	Steel	241
24	2	Aluminum	184
24	2	Titanium	210
16	2	Steel	183
12	2	Steel	153
Colander 5 mm aluminum for all cases			

Table 4: Influence of the colander thickness.

Colander thickness [mm]	Lowest EF [Hz]
5	183
4	166
3	145
2	123
5 no colander ahead of brackets	149
5 no colander ahead of 0.37 m (2 elements)	183
5 no colander ahead of 0.39 m (1 element)	178
16 brackets of 2 mm thickness for all cases	

Based on these results the investigation was carried on in more detail. A new, detailed FEM model of the bracket system was built. As a basis a model using 16 brackets was set up. In parallel a design for the attachment of the brackets to the the nose was developed and also modelled in the FEM. The initial design was to bolt the brackets directly to the nose for simplicity and making use of the low temperatures at the nose edge, which allow the use of metallic fasteners. However, after discussions concerning the possible effects of local disturbances on the boundary layer due to the bolt heads and countersunk holes possibly leading to premature tripping, that plan was dropped and an alternative solution was pursued.

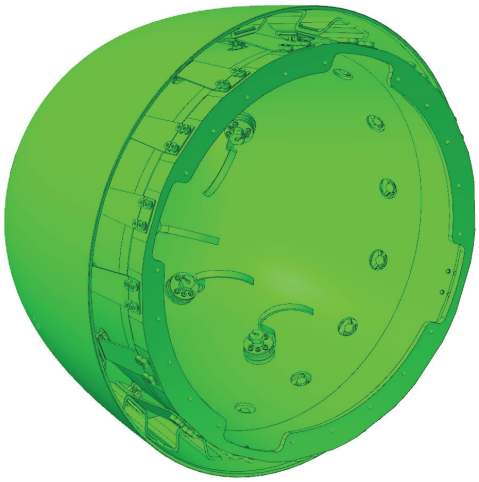

Figure 9: EXPERT nose assembly.

The design that was used in the FEM includes a C/C-SiC hat profile that is integrally joined to the inside of the nose. The metallic brackets are bolted to the top section of the hat profile. The cold end of the brackets is bolted to the colander near the edge of the colander. The complete nose assembly is shown in Fig. 9, the nose with attachments but without colander and without sensors is depicted in Fig. 10.

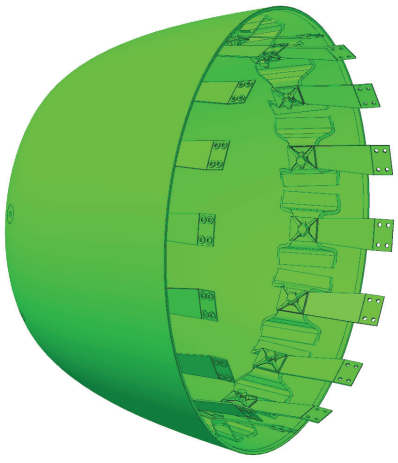

Figure 10: Nose and attachment components.

5. ANALYSIS OF THE BRACKET SYSTEM

The FEM model was built using parameters for the main geometric properties of the attachment system to conduct variation analyses and determine the influence of the individual parameters on the stiffness of the overall system. Table 5 states the geometric parameters that were variable and lists their initial values used for the basic variant.

Table 5: FE model parameters and initial values.

#	Parameter	Initial Value
1	Number of brackets	16
2	Nose thickness	6 mm
3	Colander thickness	4 mm
4	Bracket length	95 mm
5	Bracket width	40 mm
6	Bracket thickness	2 mm
7	Bracket angle to vehicle x-axis	0°*
8	Bracket distance to colander	10 mm**
9	Hat profile thickness	5 mm
10	Hat profile width	40 mm***
11	Hat profile height	25.4 mm
12	Hat profile side angle	10°
* positive angle has the bracket front end at a larger radius ** used to adjust hat profile height *** always equal to bracket width		

The model that was used for the thermal and mechanical analysis is a quarter model of a 90° sector (for the 16 brackets) using shell elements for most of the structural items, shown in Fig. 11 and solid elements for the insulation, presented in Fig. 12. If the number of brackets is changed, the sector angle is adjusted accordingly. The same model was used for the mechanical analysis. For the eigenvalue analysis the structural items of the thermal sector model were repeated in a cyclic way to arrive at a full mechanical model that accounts for all the modes.

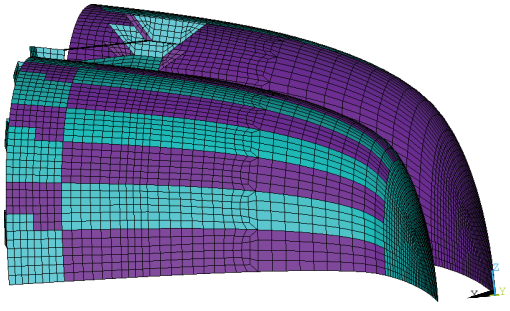

Figure 11: Structural items as shell elements.

With the basic variant a modal analysis was done and taken as the reference against which the variations were compared.

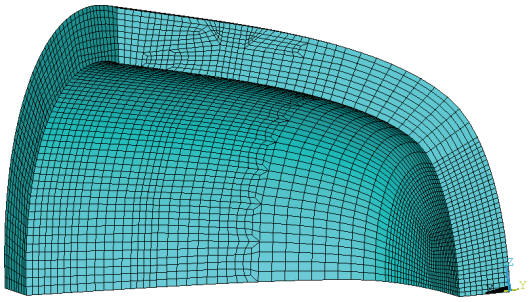

Figure 12: Solid model elements.

5.1 Modal Analysis

For the modal analysis the model was fixed to the ground (all degrees of freedom equal to zero) at the colander edge. The basic variant with parameter values according to Table 5 has the 1st EF at a value of 283 Hz.

In a variation of the parameters their influence on the global behaviour was investigated. In each variation analysis only one parameter was changed and the others held constant. In some cases the variation of one parameter, e.g. changing the bracket angle to the x-axis, meant that another parameter had also to be changed in order to keep all others at the same value.

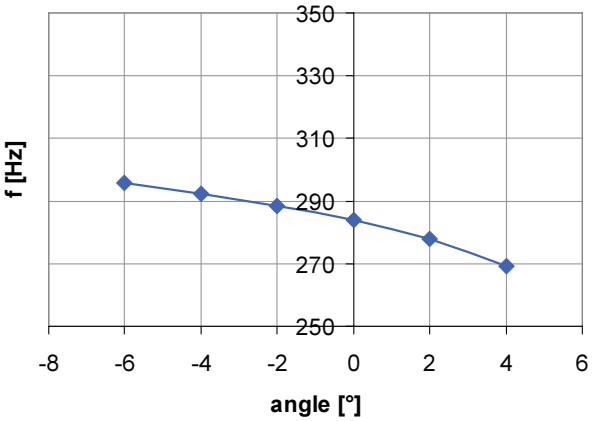

Figure 13: Influence of the bracket angle.

As an example of the parameter variations, two of them are presented in detail. In Fig. 13 the influence of the metallic bracket angle relative to the vehicle x-axis is shown. Zero angle has the bracket aligned with the vehicle x-axis, a positive angle has the bracket front end at a larger radius than the rear end. The relation is almost linear with increasing system stiffness when the angle is decreased, coming from the fact that with a negative angle, the brackets form a conical system with the larger diameter at the rear end away from the nose end. It can be seen that a slight change of the angle can increase the EF by 10 to 20 Hz.

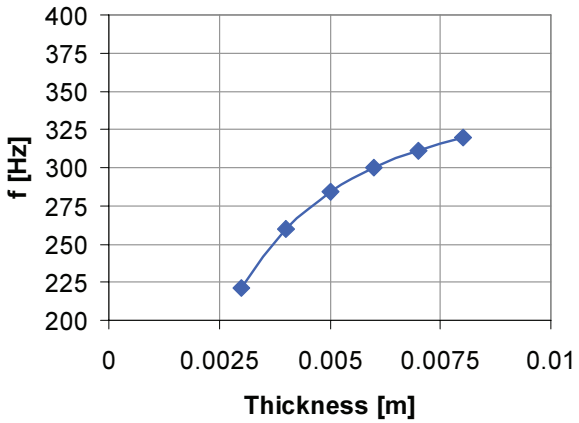

Figure 14: Hat profile thickness influence on the EF.

The second example Fig. 14 shows the dependance of the system stiffness on the thickness of the C/C-SiC hat profile. Here the relation is non-linear with rapidly decreasing EF values for thinner hat profiles. The change in the EF can be as large as 100 Hz when the thickness is changed by 5 mm. When doing these variations for optimization it has to be kept in mind that there is also a relation between the hat profile stiffness and the thermal stresses that are induced by the nose shell expansion. When all parameters are varied at the same time in the direction of better stiffness, a value of 402 Hz can be reached in comparison to Table 5 when reasonable changes are assumed. However, this variation has not been checked for the stresses due to temperature and pressure.

Table 6: Parameter values for increased stiffness with 402 Hz EF.

#	Parameter	Value
1	Number of brackets	16
2	Nose thickness	6 mm
3	Colander thickness	4 mm
4	Bracket length	85 mm
5	Bracket width	50 mm
6	Bracket thickness	2 mm
7	Bracket angle to vehicle x-axis	-3°
8	Bracket distance to colander	20 mm
9	Hat profile thickness	6 mm
10	Hat profile width	50 mm
11	Hat profile height	22 mm
12	Hat profile side angle	15°

5.2 Thermal Analysis

With the modified design and the new loads a thermal analysis was carried out with the 16-bracket design. The 3-D heat flux distribution was available for the

peak heating condition at Mach 14. The heat flux values were given as DKR values and were scaled with a factor of 0.766 to arrive at a level of a partial catalytic material as the C/C-SiC. The 3-D heat flux distribution was varied over time according to the transient load profile of the stagnation load as shown in Fig.3.

The distance between nose and colander is 50 mm and the internal volume is filled with fibrous insulation of two types. The outer layer of 20 mm for very high temperatures, the inner layer for medium to high temperatures. The nodes that were used for the evaluation of the temperatures are depicted in the Figures 15 and 16.

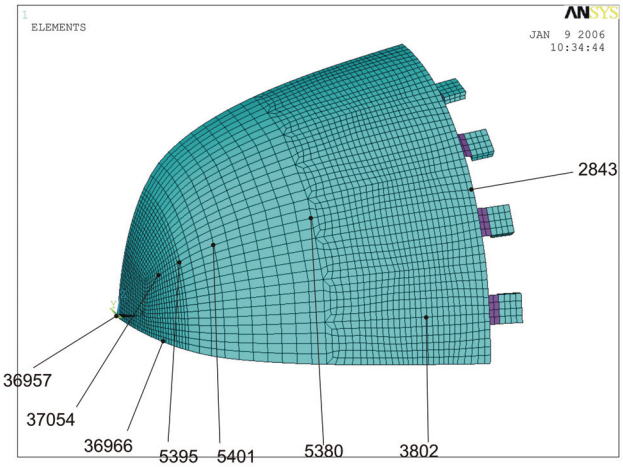

Figure 15: Surface nodes for temperature evaluation.

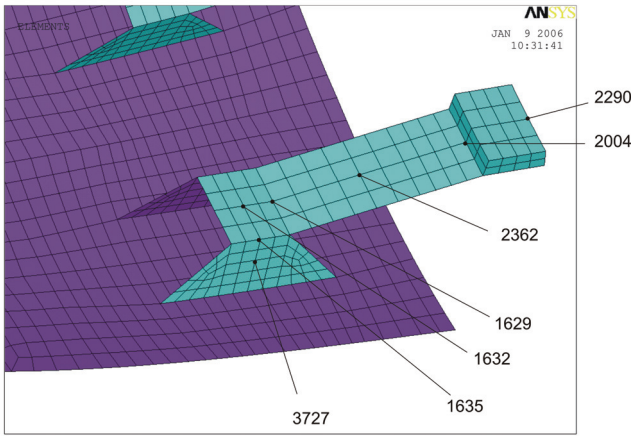

Figure 16: Attachment nodes for temperature evaluation.

The nose stagnation region temperatures that were calculated are presented in Fig. 17. Within two minutes after the heat load begins to build up the maximum temperature of 1922°C is reached. The location of the maximum value can be found not exactly in the stagnation point, but a little to the side since the heat load profile shown in Figure 6 has it´s maximum not in the very stagnation point. It can be noted that the temperatures up to the start of the bend of the nose at node 5395 are practically at the same level at 1900°C. Only at node 5401 the decreasing heat load becomes effective and the peak temperature is down to 1670°C, which is roughly at the material limit for re-usability.

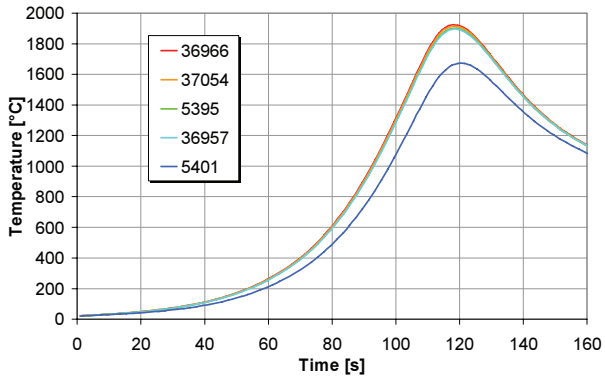

Figure 17: Nose stagnation temperatures.

The maximum temperatures in the downstream regions of the nose decrease considerably as is shown in Fig. 18. At node 5380 which is located about halfway between stagnation point and nose edge, the maximum value is merely 1330°C, at node 3802 which is located at the hat profile station it is 827°C and at node 2843 at the edge the nose should be glowing at 728°C.

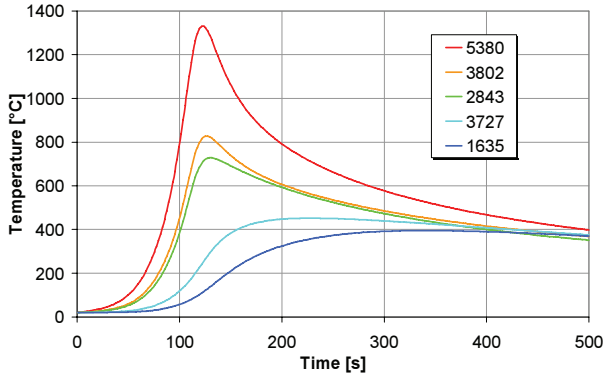

Figure 18: Nose edge and hat profile temperatures.

The internal components of the attachment system are in part an integral component of the nose and made of C/C-SiC, but they are also made of Inconel in the case of the bracket and therefore also a temperature of a couple of hundred degrees could be critical in conjunction with high mechanical loads. Temperature conditions for those components are given in Figures 18 and 19. In Fig. 18 the nodes 3727 and 1635 of the C/C-SiC hat profile are contained with maximum temperatures of 452°C and 395°C respectively.

In Fig. 19 the temperatures of the metallic bracket at the interface to the hat profile are illustrated. Node 1632 is located in the center of the hat profile top section where the temperature reaches a peak of 378°C. Node 1629 represents the end of the hat profile top section; here a

value of 357°C could be registered. Node 2362 at the midway loaction between hat profile and colander was at 150°C and still rising in temperature at the analysis end time of 500 seconds. The colander temperatures exhibit a very small increase in temperature.

The most important result of the thermal analysis was that the temperatures in the metallic bracket can be handled well by the Inconel material, without properties decreasing. This was especially important since the brackets are loaded by compression in a possible buckling situation.

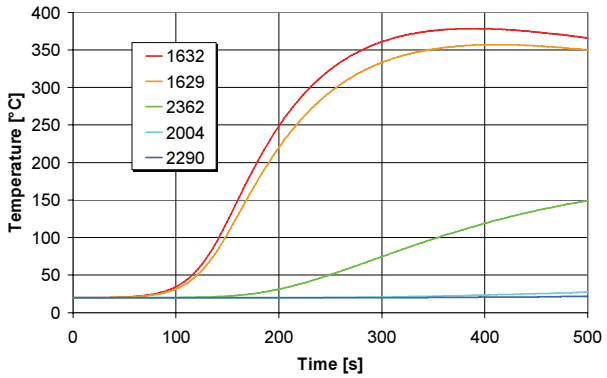

Figure 19: Temperatures of the metallic components.

5.3 Mechanical Analysis

For the mechanical analysis it had to be determined which of the revised loads were the dimensioning cases. It was found quickly that for the nose of EXPERT the re-entry load case with a quasi-static deceleration was the most critical one. This is due to the fact that the deceleration is caused by the aerodynamic pressure and drag on the surface of the vehicle and these loads have to be transferred by the nose and the metallic TPS. Since the nose and the TPS are the reaction surfaces for these loads the resultant inertial load of the complete vehicle mass has to be transferred via those components and their respective load introduction elements. When in a rough estimation the vehicle mass of 400 kg is considered under a quasi-static deceleration level of 17g the resulting forces are close to 67 kN.

Load Determination

A more detailed evaluation of the load conditions had to establish a suitable approach for the determination of the correct share of the deceleration load between nose and TPS. It had to attribute the fact that the aerodynamic loads show a distribution with large differences in their absolute values with the main share acting on the nose.

The approach that was selected is outlined in Fig. 21 and was based on analyzing two different pressure distributions on two different FE models as shown in Fig. 20 and to determine the resulting reaction forces for each of them. The first was a model of just the nose with the relevant pressure distribution as load. The second was a simplified model of the the complete vehicle, i.e. nose and TPS surface with the pressure distribution all over the vehicle. The simplified model was the nose plus a conical extension with the half-angle of the real vehicle conical surfaces, excluding the cut-away areas and flaps of the real vehicle. In each case the reaction loads were determined. The difference in the reaction loads was then the amount of deceleration load that could be carried by the TPS. In addition, for the determination of the correct value of the loads acting on the nose load introductions, it had to be considered that the nose assembly mass of roughly 50 kg can not be taken into account into the mass to be decelerated. Drag effects due to skin friction were calculated from available skin friction coefficients with 600 N for the whole vehicle. Since that is small compared to the forces due to pressure loads and difficult to assess because the effect of the flaps producing additional drag was not considered, the friction was neglected.

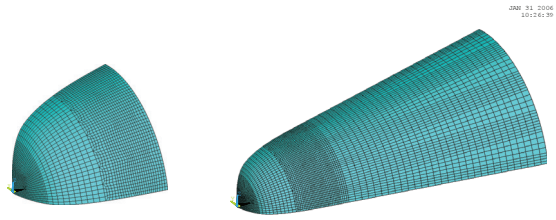

Figure 20: FE models used for load determination.

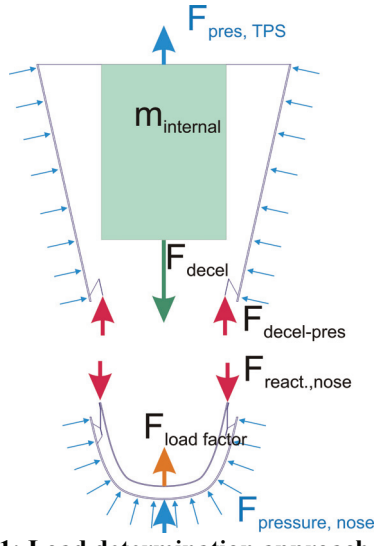

Figure 21: Load determination approach using the pressure distribution on nose and TPS.

Due to these simplifications the reaction forces are lower than the expected inertial forces of that mass. The reaction force with the nose model only was found to be 23783 N, the value for the full length model was 28857 N; hence the difference was 5074 N or the share of the load taken by the nose is 82%. The reaction force of the vehicle without nose assembly – i.e. the reaction load

acting on the load introduction components at the interface between nose and vehicle – was calculated with 350 kg and a load factor of 16.8 to be 57683 N. From this value 5074 N were deducted, arriving at 52609 N. Then a scaling factor was applied on the values of the pressure distribution on the nose model and the resulting reaction load in that model was checked. The scaling factor was adjusted until the reaction load in the nose model was 52609 N. The corresponding scaling factor was approximately 2.1 which corresponds to the 16.8 g load factor. The analyis that was first carried out and is presented in the following still used a scaling factor of 3.4 due to an overly conservative assumption on the load conditions. Therefore the pressure influence is overstated in the following. However, since the pressure scaling factor of 3.4 is roughly equivalent to a load factor of 24, it supports the view that even the landing impact with a shock of 23 g can be handled.

The scaled pressure loads were used as the input for the mechanical analysis of the nose system in a static analysis as shown in Fig.22.

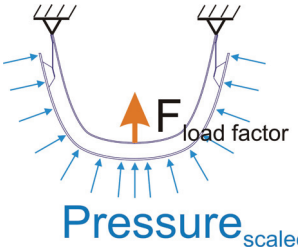

Figure 22: Final model with scaled pressure load.

Stress Evaluation

The evaluation of the results was done with two principal objectives. First, the margins of safety of the structural components were to be determined. Second, the displacement of the nose edge over time was of great interest, since it determines the conditions at the gap between the CMC nose and the adjacent metallic PM1000 TPS. For the metallic components the evaluation was based on a classic von Mises approach, for the C/C-SiC material the evaluation looked for the maximum stresses in tension, compression and shear.

The results of the thermal analysis were used as input for the mechanical analysis to induce the thermal strains and control the material behaviour of such materials that exhibit temperature dependent properties. At a given time of the trajectory that was to be analyzed, the pressure distribution was applied for that time and the temperature field from the thermal analysis was read in as thermal load. The task was to evaluate the combined stresses at any time of the transient load profiles to determine any critical condition, which may not even occur at peak external load level but at a later time due to internal temperature storage with reversed effects compared to peak loading condition.

The maximum stresses for the C/C-SiC nose were found in the load introduction elements of the hat profile. They have a value of 78 MPa and occour at peak pressure shortly after peak heating at the rear end of the side flanges of the hat profiles as shown in Fig. 23. A comparison with the pure thermal stresses of 46 MPa shown in Fig. 24 reveals that the added mechanical load from the pressure changes the stress distribution in the hat profiles by reducing the stress level at the front end of the side flanges and increasing it at the rear end.

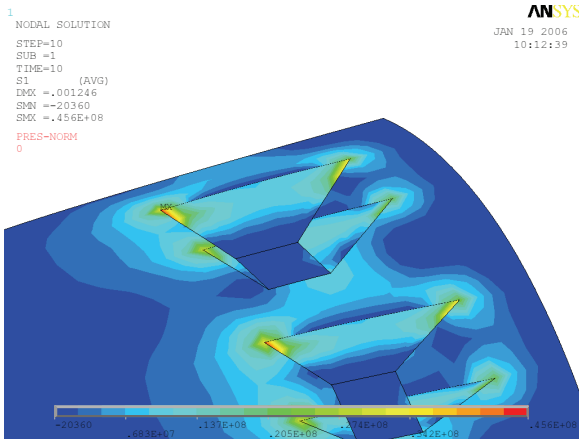

Figure 23: Maximum stresses due to temperature load.

The stress of 78 MPa in the hat profile is practically the yield stress for the standard material quality C/C-SiC XB, which is 80 MPa as described in Table 7.

Table 7: Properties of different C/C-SiC types.

Strength	C/C-SiC XB	C/C-SiC XB T800	C/C-SiC XT
Tensile [Mpa]	80	120	190
Compression[MPa]	225	205	205
Shear [MPa]	54	60	60

Therefore, if a factor of safety of 1.5 shall be applied and a positive margin of safety shall be obtained, the material has to be exchanged for a higher quality with higher yield value. The C/C-SiC XB T800 uses a better fibre and exhibits 120 MPa yield in tension, which is just enough for this situation. There would be the possibility to choose a material with an even better quality, the XT standard with a yield value of 190 MPa. The exchange of the material types is affecting mainly the fabrication and has no other influences on the use properties, except for strength.

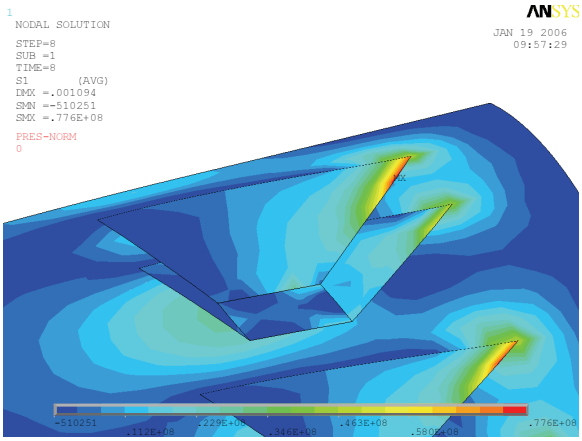

Figure 24: Stresses due to combined thermal and pressure load at max. pressure.

The metallic brackets that are attached to the hat profiles of the nose experience higher stresses, but have also higher allowables. Most of the brackets is loaded with roughly -50 MPa, at the interface to the hat profiles there are concentrations of up to -230 MPa. Fig. 25 shows the von Mises evaluation.

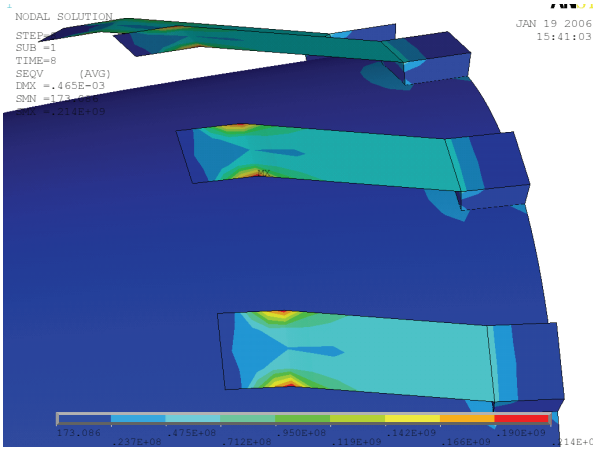

Figure 25: Stress distribution in the brackets at peak pressure.

Margins of Safety

From the stress evaluation the margins of safety were determined for the individual components on the basis of the allowables for the C/C-SiC XB T800 given in Table 7.

From Table 8 it can be noted that the hat profiles and the metallic brackets have the smallest margins of safety with +0.02 and +0.18 respectively. The nose shell itself is well in the positive range and the colander and related components are in fact oversized.

Table 8: Margins of safety.

Component	Yield [MPa]	Stress [MPa]	FoS	MoS
Nose shell	-225 / 80 C/C-SiC XB	-28 +30	1.5	+4.35 +0.77
Hat profile	-205 / 120 C/C-SiC XB T800	-50 +78	1.5	+1.73 0.02
Metallic Bracket	414 – 621 tensile RT Inconel 625	+50 -233	1.5	7.28 +0.18
Colander/ bracket I/F-block	530 tensile RT Steel	-55	1.5	+6.42
Colander	530 tensile RT Steel	+50	1.5	+6.1

Displacement Evaluation

The nose edge displacement is of great importance. With the transient displacement of the metallic TPS front edge it determines the step height at the interface between the two systems. As a requirement, the step height from nose to TPS must never be positive – which means an upward step in flow direction - to avoid the formation of local stagnation points with overheating. On the other hand, also a large negative step is not desirable, since it can lead to early transition to turbulent flow.

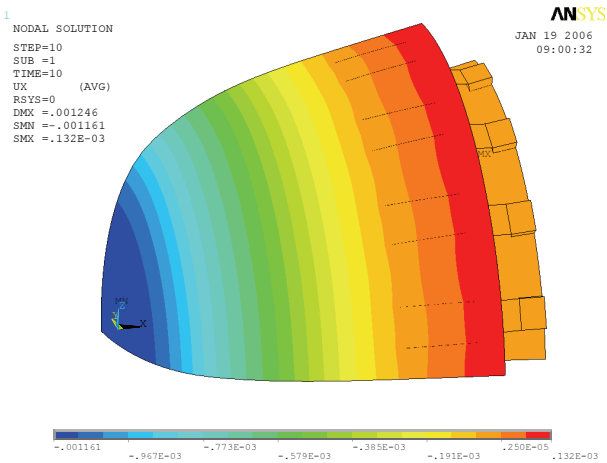

Figure 26: Axial displacement at maximum temp.

The maximum thermal displacement in axial direction is observable in the stagnation point. It is given as negative value of x in Fig. 26 of roughly 1.1mm, which means that it is an extension of the nose in flight direction; positive x-axis pointing from the nose to the base of the vehicle. The axial displacement at the nose edge is a mere 0.13mm in positive direction, to the base of the vehicle, meaning the gap between nose and TPS will be narrowed.

When the pressure load is added to the thermal load as to be seen in Fig. 27 the displacement picture changes only gradually. The biggest effect can be seen in the stagnation region with the highest pressure where the deflection is reduced by 0.5 mm. The areas towards the edge are hardly affected by the pressure with respect to displacement.

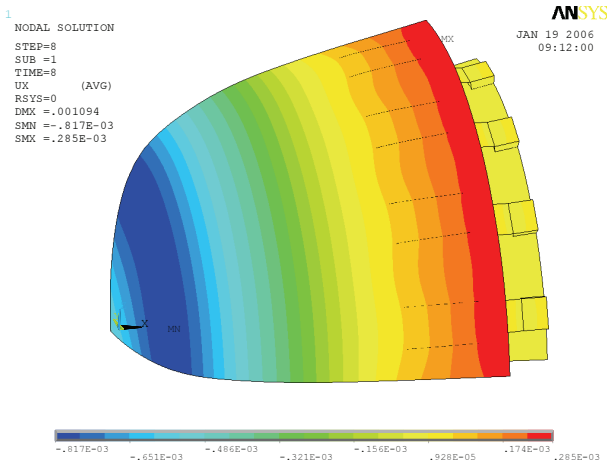

Figure 27: Axial displacement under combined load at maximum pressure.

The largest radial displacement can be observed at a location around the bend of the nose. The nose radius in this area will be larger by 0.8mm and the pressure load makes almost no difference on the deflection values, it only slightly increases maximum radial deflection around the nose bend.

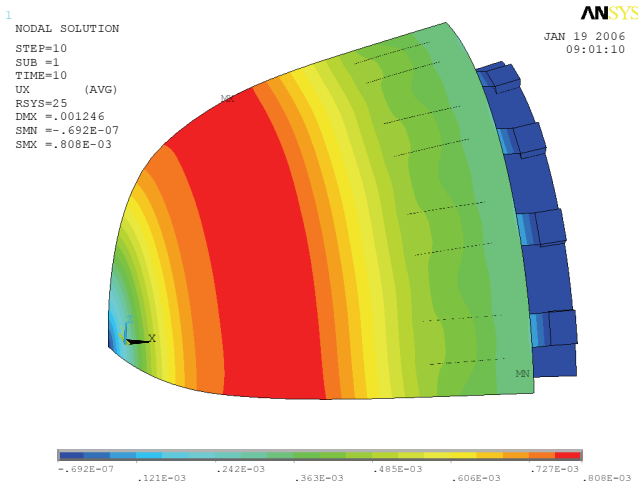

Figure 28: Radial displacement at maximum temp.

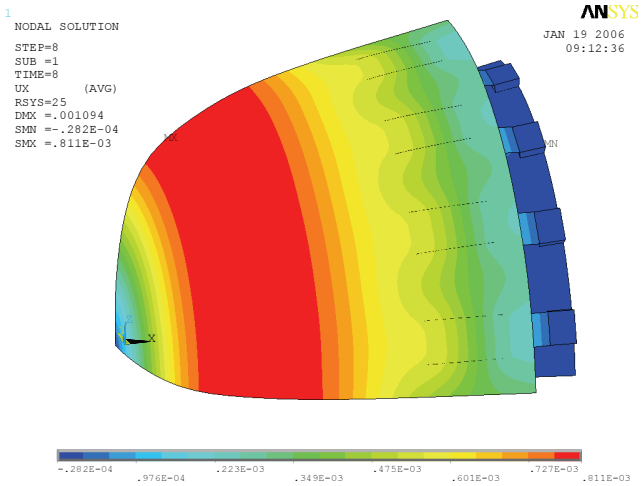

Figure 29: Radial displacement under combined load at max. pressure.

The time dependent edge displacement under combined load as one of the determining parameters for the step geometry at the nose/TPS interface is shown in Fig. 30 for both components, axial and radial displacement.

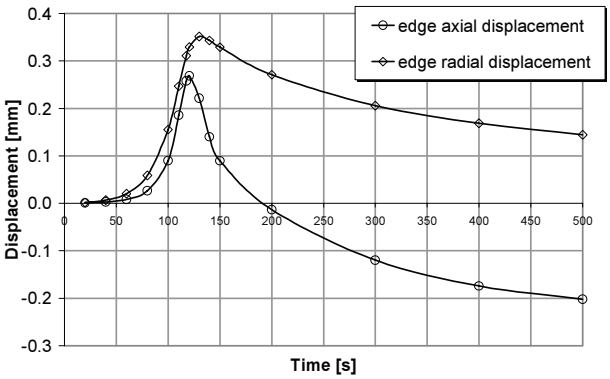

Figure 30: Nose edge displacements over time.

6. CONCLUSIONS

As the development of EXPERT is going on with a lot of issues still in a progressing and changing phase, the findings described may be regarded as a status description, however, not far from the final set of data that will be valid for the flight vehicle since the results indicate that the proposed design will be able to fulfil all the targeted objectives. Many of the issues related to the nose design were not reported in detail or not at all. For instance the types of payloads with their sensors that will be integrated into the nose shell was not touched. This is the case because the emphasis was on the discussion of the specific issues of the use of a CMC component in the EXPERT environment. The application of a CMC component for the stagnation heat shield of a ballistic entry vehicle might at first seem to be unusual because the material is mainly associated with technology developments for re-usable systems. But when the objectives of the mission are looked at, with the multitude of high-fidelity measurement tasks to

be performed around the vehicle, the motivation for the selected approach is becoming very strong. In contrast to an ablative thermal protection system the C/C-SiC solution has to offer a lot of advantages with regard to a clean flow over the capsule surfaces. The amount of surface degradation that will be observable on the C/C-SiC nose after flight will be very small, and is a minor issue compared to the advantages that will be achieved.

7. REFERENCES

[1] Reimer, T., "The EXPERT C/C-SiC Nose Cap – System Design and Thermomechanical Layout", AIAA-Paper 2005-3262, AIAA-CIRA 13th Space Planes and Hypersonic Systems Conference, May 16-20, 2005, Capua, Italy

[2] Laux, T., „Untersuchungen zur Hochtemperatur-oxidation von Siliziumkarbid in Plasma-strömungen", Dissertation, Institute of Space Systems, Stuttgart University, Germany, 2004

[3] Curry, D. M., "Space Shuttle Orbiter Thermal Protection System Design and Flight Experience", 1st ESA/ESTEC Workshop on Thermal Protection Systems, 1993, Noordwijk, ESA/ESTEC

[4] Tigges, M., "Preliminary V-201 Entry Flight Profile with Landing Site Precision. Cycle 8", NASA, 1998, October, Technical Report

[5] Voinov, L.P., "Thermal Designing of the BURAN Orbital Spaceship", Aerospace Systems: Book of Technical Papers, 1997, 115-122, Lozino-Lozinsky, G.E., Bratukhin, A.G., Publishing House of Moscow Aviation Institute, Moscow

[6] Weihs, H., Hald, H., Reimer, T., Fischer, I., "Development of a CMC Nose Cap for X-38", IAF-01-I.3.01, 52 International Astronautical Congress, Toulouse, 1.-5. October 2001.